Luminescence of Nanodiamond Driven by Atomic Functionalization: Towards Novel Biomolecular Detection Principles

Vladimíra Petráková[1], Andrew J. Taylor[2], Irena Kratochvílová[2], František Fendrych[2], Jiří Vacík[3], Jan Kučka[3], Petr Cígler[4], Miroslav Ledvina[4], Anna Fišerová[5], Peter Kneppo[1] and Miloš Nesládek[5]

[1]Czech Technical University in Prague, Faculty of Biomedical Engineering, Sítná sq. 3105, 272 01 Kladno, Czech Republic

[2]Institute of Physics, Academy of Sciences of the Czech Republic, v.v.i, Prague 8, Czech Republic

[3] Institute of Nuclear Physics, Academy of Sciences of the Czech Republic, v.v.i, 250 68 Rez near Prague, Czech Republic

[4] Institute of Organic Chemistry and Biochemistry, Academy of Sciences of the Czech Republic, v.v.i., Flemingovo n. 2, 166 10 Prague 6, Czech Republic

[5]Institute of Microbiology, Academy of Sciences of the Czech Republic, v.v.i., 142 20 Prague 4, Czech Republic

[6]IMOMEC division, IMEC, Institute for Materials Research, University Hasselt,

Wetenschapspark 1, B-3590 Diepenbeek, Belgium

vladimira.petrakova@fbmi.cvut.cz, taylor@fzu.cz, krat@fzu.cz, fendrych@fzu.cz, vacik@ujf.cas.cz,

kucka@ujf.cas.cz, cigler@uochb.cas.cz, ledvina@uochb.cas.cz, fiserova@biomed.cas.cz, kneppo@fbmi.cvut.cz, milos.nesladek@uhasselt.be

RECEIVED DATE (to be automatically inserted after your manuscript is accepted if required according to the journal that you are submitting your paper to)

CORRESPONDING AUTHOR FOOTNOTE Vladimíra Petráková, vladimira.petrakova@fbmi.cvut.cz, +420 224 359 901, +420 737 107 731

ABSTRACT

High biocompatibility, variable size ranging from ~ 5 nm, stable luminescence from its color centers and simple carbon chemistry for biomolecule grafting make nanodiamond (ND) particles an attractive alternative to molecular dyes for drug-delivery. Here we present a novel method for remote monitoring of chemical processes in biological environment based on color changes from photo-luminescent NV centers in ND. We propose to drive the NV luminescence chemically, by alternating the surface electric field developed by interacting atoms and molecules with the diamond surface. Due to the small ND size, the developed electric field penetrates into the bulk of the nanoparticle and intermingles with the electronic NV states. Our technique has advantages over FRET (Foerster Resonance Energy Transfer) for which the sensitivity to size scales as $1/r^6$. In our method, due to Columbic charge interactions and spherical particle size effect, luminescence effects are observed up to ~ 20 nm in depth, compared to size < 5 nm for FRET. This allows construction of optical chemo-biosensors operating in cells, visible in classical confocal microscopes. We demonstrate this phenomenon on oxidized and hydrogenated ND as well as single crystal diamond containing engineered NV centers. Hydrogenation of NDs leads to quenching of luminescence related to negatively charged (NV^-) centers and by this way produces color shifts from NV^- (636 nm) to neutral NV^0 (575nm) luminescence. We model how the reduction of

diamond size increases the magnitude of NV color shift phenomena.

KEYWORDS nanodiamond, nanoparticles, luminescent centers, NV, surface functionalization, molecular imaging

MANUSCRIPT TEXT

Recently Ho and co-workers demonstrated the use of nanodiamond (ND) particles for delivering therapeutic agents in-vivo[1]. ND particles with a size range of 5-100 nm can also serve as a new type of optical marker for cellular imaging[1-4]. Strong ND photoluminescence (PL) originates from single photon producing nitrogen-vacancy (NV) color centers consisting of a substitutional nitrogen atom next to a vacancy, engineered artificially in the diamond lattice. The nanoscale effects related to artificially engineered NV color centers, attracted important attention to diamond due to applications ranging from quantum computing to cell-imaging[2-4]. The luminescence from NV centers is extremely stable without any photobleaching or photoblinking[5-7] and compared to more known quantum dots, ND brings additional advantages such as high biocompatibility[8-9] and simple C-surface chemistry[10,11]. This allows grafting of biomolecules that are interesting for the cellular targeting[12,13] or biomolecular drug delivery[14-16].

In this article we describe how the nm-size and surface chemistry-based effects can make the ND bulk luminescence sensitive to chemical processes ongoing at the ND surface, aiming at using ND for monitoring the chemical environment such as surface charges/pH, cellular DNA/RNA hybridization, interaction with cell receptors, etc. Our method is based on the electrical field developed in a close proximity of ND surfaces, penetrating into the ND grain and influencing the occupation of the luminescent NV centers, that exist in neutral (NV^0) or negative charge states (NV^-)[17,18] with different PL properties and changing emissions wavelength, i.e. 575 nm for NV^0 and 636 nm for NV^-. This method explained below yields advantages over recently demonstrated ND FRET[19] (Foerster Resonance Energy Transfer) scaling as $1/r^6$, allowing to induce luminescence shifts originating at energy transfer between

ND donor and acceptor dye of size ~ 5 nm. In our case, due to $1/r^2$ Coulombic interactions, we can observe chemically driven luminescence shifts up to larger distances ~ 20 nm in depth, which is exactly calculated by modeling. This allows construction of optical chemo-biosensors with sizes of about 40 nm operating in cells and easily visible in classical confocal microscopes. This can be especially interesting for drug delivery research and for monitoring chemical interactions occurring in cells based on covalent or non-covalent interactions with charged molecules such as DNA and by various surface terminations. We demonstrate this mechanism on ND with hydrogenated and oxidized surface which exhibits important differences in the surface electrical potential. We validate the model and ND size effect by comparing the results with a defect-free, chemical vapor deposition (CVD) grown single crystal diamond (SCD) which was implanted in nm depth with nitrogen and subsequently annealed to convert N to NV centers by trapping of vacancies. Electric filed penetration related and corresponding size effects of ND particles on luminescence is modeled mathematically. We show clearly why the size effect of nanoparticles is important with comparison to bulk SC CVD diamond[20, 21] as this allows an increase significantly in the color shift magnitude.

Results and discussion

Quenching of NV^- luminescence on ND particles

H-terminated diamond surfaces[22,23] possess a high electrical dipole moment which attracts polar ions such as water adsorbates, leading to upwards surface band bending, causing an 2 dimensional hole gas (2DHG) conductive surface and pinning of the Fermi level at the valence band maximum (E_{VBM}) [24,25]. , an effect called the surface transfer doping[22]. We propose to use this effect to induce changes in the occupation of NV^0 and NV^- centers laying in the band-bending zone. NV^0 and NV^- centers, have different ground state energy levels 1.2 eV and 2.0 eV (calculated by Goss et al.[26,27]), which enables proposed selective occupation. Specifically, if Fermi level (E_F) energy will be lowered below the level of NV^- (NV^0), the state becomes unoccupied leading to changes in the luminescence. By this way a

controlled band banding at diamond surface can target one or even both types of NV charge states. Color shifts in diamond affected by surface termination reported by our group[28] were also recently observed by an US group[29] but their origin, which we model, was not explained. In general, (A) hydrogen termination of diamond leads to upwards band bending, i.e. the hole accumulation layer, while (B) oxygen termination causes an opposite effect, i.e. downwards band bending. If the particles are sufficiently small, i.e. in ~ 10 nm scale, the electric field could influence the NV luminescence in the whole particle, leading to optically detected luminescence shifts via relative shift of NV^0/NV^- levels with respect to the E_F (i.e. the state occupation). The situation is illustrated in Figure 1.

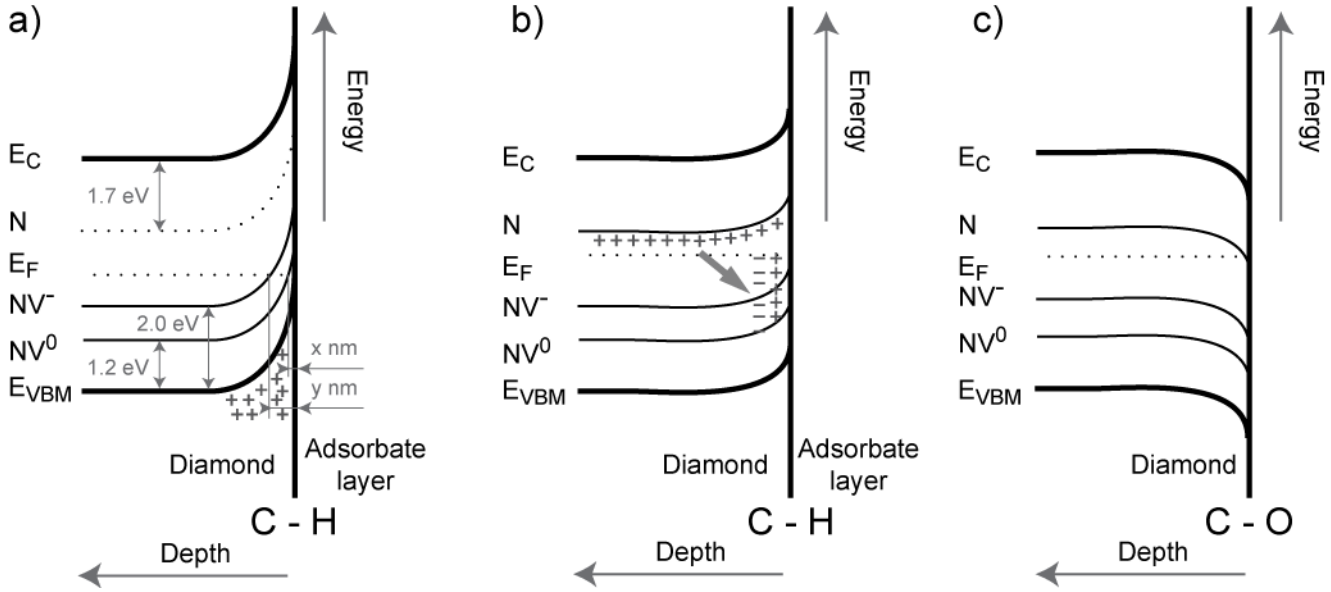

Figure 1. *Schematic model of surface band bending for hydrogen terminated diamond containing NV centers with (a) low content of nitrogen, (b) high content of nitrogen. Nitrogen in the diamond lattice acts as an electron donor, electrons will compensate the positive charge at the surface, effectively reducing the surface band bending and inhibiting the influence of hydrogen termination on photoluminescence. Additional nitrogen influences the position of the Fermi level E_F in the band gap. (c) Oxidized diamond surface with downward band bending, NV^0 and NV^- are occupied. x (nm) and y (nm) are regions of which the Fermi level crosses the NV^- and NV^0 energy, i.e. regions where the*

ground levels of NV^- and NV^0 are not occupied and therefore luminescence cannot occur.

PL in ND

Particles in 20-40 nm size, made of High Pressure High Temperature (HPHT) synthetic diamond are very suitable for biologic applications due to possibility of production of a high amount of stable NV centers. These provide sufficient luminescence contrast that is comparable to other biomarkers, and retains advantages related to their nano-dimension. To investigate the effect of PL shifts, HPHT ND particles containing approximately 200 ppm of N and with a peak size distribution at ~ 40 nm were irradiated by protons using energy of 5.4 MeV to produce vacancies and subsequently annealed at 700°C (see experimental details) to produce NV centers. Figure 2a shows the experimental data obtained for ND for 4 different situations: oxidized surface, hydrogenated surface of larger particle (40 nm), hydrogenated surface of smaller particle (20 nm) and diamond after subsequent oxidation performed by annealing at 400°C in air. According to our model, explained in detail in the supporting information, the NV^- luminescence with zero phonon line (ZPL) at 638 nm is fully quenched after hydrogen termination, while the NV^0 luminescence is still visible. For very small particles, the NV luminescence can be fully quenched. The NV^- luminescence can be restored again by annealing in air (leading to oxidized surfaces). Further on, Figure 2b shows the PL spectra taken at room temperature of H-terminated ND upon heating in air at gradually elevated temperature (see Materials and methods). A reverse process, i.e. backward transition from NV^0 luminescence to NV^- dominated luminescence can be generated upon heating (Figure 2b). The first change occurs at about 200°C. This temperature agrees well with the experimentally observable desorption of adsorbates[30] confirmed by the loss of the 2DHG surface conductivity (i.e. band bending). At 400°C permanent changes in the surface termination occur leading to the loss of surface hydrogen due to oxidation, leading NV- to dominate the PL spectra. We demonstrate this effect using a confocal microscope with a single particle resolution (Figures 2c – f).

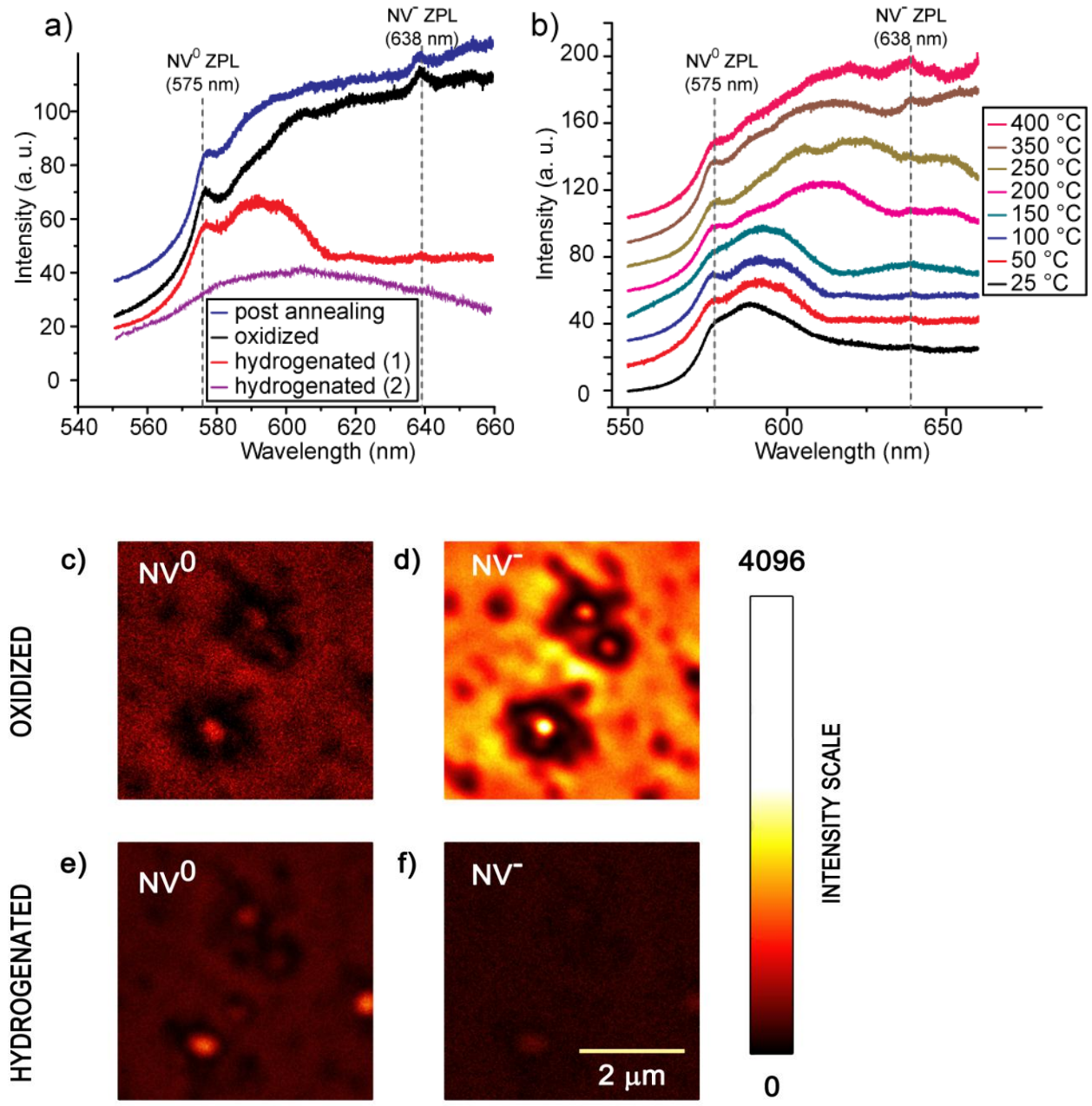

Figure 2. *Changes in NV⁻ and NV^0 luminescence induced by various terminations of 20 and 40 nm sized ND particles. (a) Spectra of oxidized, hydrogenated, and annealed surfaces at 400°C (leading to restoration of original surface termination). The hydrogenation of larger particles (~40 nm) resulted in luminescence shift towards NV^0 luminescence (hydrogenated 1), for the smaller particles (< 20 nm), the luminescence quenched completely (hydrogenated 2). (b) Luminescence changes of hydrogenated ND (40 nm) upon annealing in air at different temperatures. Samples were heated to the target temperature*

(using a ramp of 25°C per minute), kept at the set temperature for 30 minutes and then cooled down to the room temperature. All spectra were taken at room temperature and baseline corrected.

Figure 2c.-f. Confocal image of single ND particles upon various treatments. For oxidized ND, both NV^0 (c) and NV^- (d) luminescence is clearly visible in contrast to hydrogenated ND, where NV^0 luminescence (e) is dominant and NV^- luminescence (f) is barely visible. Confocal PL images correspond to luminescence collected from 570 nm to 610 nm spectral range for NV^0 and from 630 nm to 750 nm for NV^-.

Investigation of PL from NV centers implanted to different depths

To verify how the ND compares to high purity single crystal diamond (SCD) with the defined bulk properties, we have used low energy ion implantation (1 - 6 keV), to produce NV centers in a defined depth and to study its influence NV color shift changes. Four different sectors in a high purity SCD were shallow implanted with nitrogen, using energies 1 keV and 6 keV. Created NV centers were localized from around 3 nm to 10 nm of depth (See Material and methods). Surface of the SCD was later oxidized and hydrogenated.

Figure 3 shows typical Raman and PL spectra of hydrogenated and oxidized SCD for implantation energies 1 and 6 keV. Though the NV^-/NV^0 ratio changes clearly with the surface termination, the observed changes are significantly lower than that observed in ND particles. PL emission from NV^- ZPL is also clearly influenced by the implantation energy. For H-terminated SCD on sectors with 6 keV implantation energy (and higher surface conductivity), PL spectra showed decreased emission from NV^- ZPL compared to 1 keV implantation (Figure 3a). To explain the reduction of the effect compared to ND we have performed exact mathematical modeling of the effect.

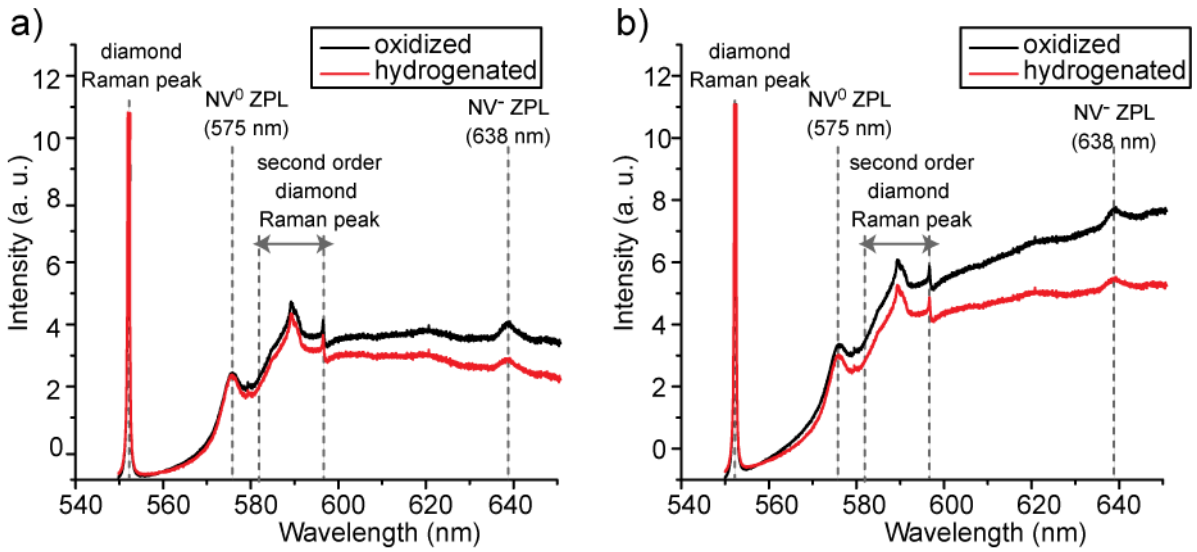

Figure 3. *514 nm-pumped Raman and PL spectra of treated SCD, showing the influence of different surface termination on NV^0 and NV^- related luminescence. NV^0 ZPL (575 nm) peaks and NV^- ZPL (638 nm) peaks are visible for oxidized SCD. For SCD with hydrogenated surface, NV^- related luminescence is decreased with an increase in NV^0 related luminescence. All spectra are normalized to the sp^3 carbon Raman peak (1332 cm^{-2}) and background corrected. a) 1 keV and b) 6 keV N^+ ion implantation energy.*

Band bending model calculations

The optical excitation of NV^- or NV^0 ground states, can only occur by absorbing a photon if the NV^0 or NV^- ground states were originally occupied by a single electron (neutral NV^0) or two electrons (negative NV^-). That means, E_F must lay above the dark ground level of particular NV^0 or NV^- for the center to be visible in PL (with an exception of the charge transfer from other defects). Compared to the simple 2DHG band bending model in H-terminated diamond[22], when working with diamond containing nitrogen and NV centers, one has to take into account the additional influence of NV^- , NV^0 and N defects. These defects will contribute to the total charge balance and influence the surface band bending (see Figure 1). If the concentration of the donor like centers (N or NV^-) is increased, the positive charge at an H-terminated surface can be partially compensated, converting N to N^+ and NV^- to NV^0. The upwards band bending can be then consequently reduced[31], depending on the concentration of

adsorbates.

In our model, the occupation of NV^0 and NV^- states was calculated from the Boltzmann's distribution, taking into account the presence of N and NV centers at various concentrations. The electric field profile on an H-terminated surface with surface adsorbates is calculated using the Poisson equation for a dielectric medium, the space charge density at the diamond surface and also depth profiles for N and NV. The values for NV^0 and NV^- energy levels (1.2 eV and 2.0 eV respectively), relative to the valence band top, were taken from reference Goss et al.[26,27]. N acts in the model as a deep electron donor with energy level at 1.7 eV below the conduction band[31] (Figure 1). The detailed model of surface band bending is described in the supporting information including an explanation of used equations and constants.

The results of the numerical simulation for the case of the H-termination of diamond containing N and NV centres are shown in Figure 4. Electrons are transferred from the valence band to surface adsorbates and generate a surface hole accumulation layer and an upwards surface band bending. The calculated value of about 2 eV for zero NV/N concentrations agrees well with the measured value[32]. However, if additional donors (N, NV^-) are available near the surface, the band bending is reduced.

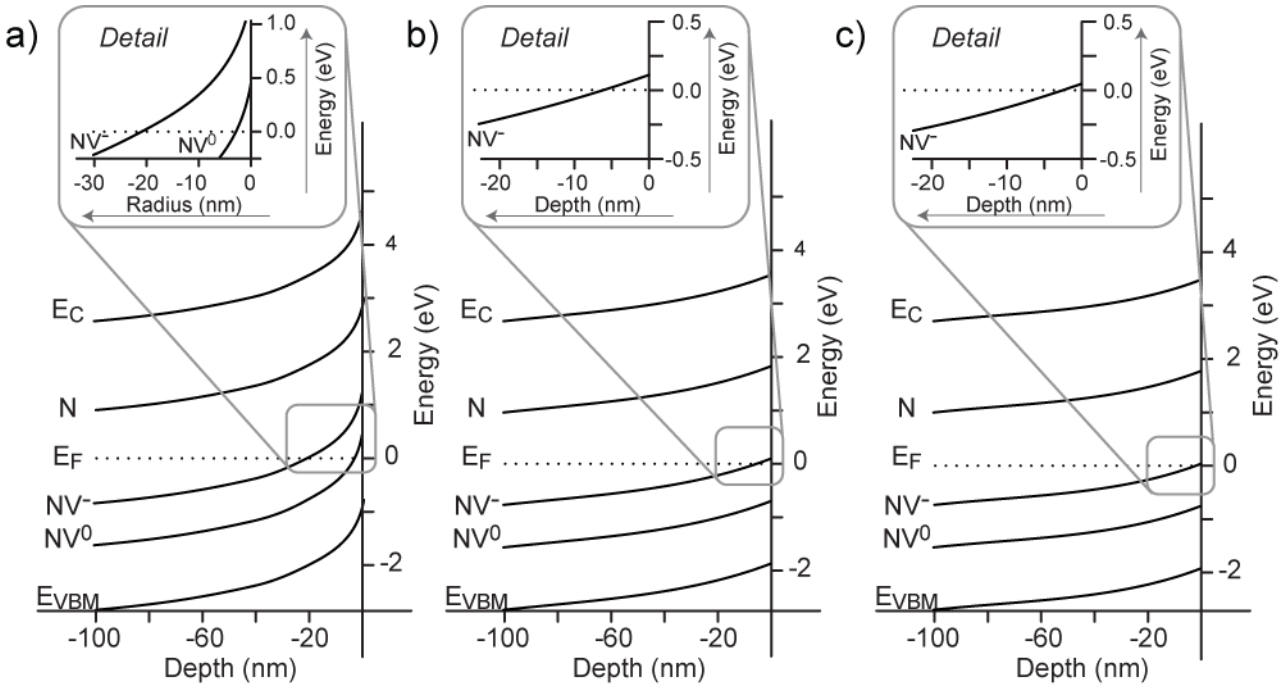

Figure 4. *Simulation of electron statistics in hydrogen terminated surfaces using density of states (DOS) model. Band diagrams show energetic profiles of the conduction band minimum (E_C), valence band maximum (E_{VBM}), NV^-, NV^0 and N impurities relative to the Fermi level (at zero energy) for (a) Ib HPHT diamond contained 200 ppm of nitrogen with surface carrier density 10^{13} cm^{-3}, where 10 % of nitrogen is converted to NV centers. This figure represents ND particles used in the experiment. In this case, we use a model using spherical coordinates, showing energetic levels as a function of radius of an ideal spherical particle (see text for details). (b) IIa diamond implanted with nitrogen (6 keV, 10^{13} ions·cm^{-2}), surface carrier density 10^{13} cm^{-3} with 1 % yield of conversion to NV centers[33,34]. (c) IIa diamond implanted with nitrogen (1 keV, 10^{13} ions·cm^{-2}), surface carrier density 10^{13} cm^{-3} with 1 % yield of conversion to NV centers. Band bending is reduced due to the presence of a deep electron donor, nitrogen, which is reducing the surface hole accumulation layer.*

Size effect of ND

Figure 4 compares band-bending calculations, for two model situations, for HPHT NDs and for implanted SCD. When comparing modeled data in Figure 4 and experimental data in Figure 2 and

Figure 3, it is clear that the observed effect of PL shift is much weaker in SCD then in our ND. Work of influence of H/O termination on PL in implanted SC CVD diamond was discussed in our previous works[21] and also recently in[20].

There are two reasons for the magnification of the surface band bending in ND compared to SCD. Firstly N is homogenously distributed in the ND particle and the conversion efficiency N to NV is higher (vacancy migration during annealing for ND[35]). Additionally, in the case of particles, there is an important size effect not considered yet. Specifically in the case of the band bending in SCD as a function of the depth (i.e. in one dimensions), the electric field was calculated using an H atom coverage and charge adsorbate densities. However if we consider spherical shaped ND particles, a 3D model must be used to solve Poisson equations. To describe this situation we have used spherical coordinates and placing one or more NV centers homogeneously distributed in the ND particle. Taking an example case of a round ND particle (in our case cubo-octahedron ND particles are rounded by oxygen etching) and placing just one NV center in the center of the sphere; leads to the signal enhancement compared to a flat single crystal diamond plate[20]. This enhancement leads to quenching of NV- luminescence up to 22 nm of depth in comparison with just a few nm for the case of SCD (shown in detail on Figure 4). This situation is modeled in detail in the supporting information, clearly indicating profound band bending and occupation changes for ND particles compared to SCD.

Conclusions

Luminescent properties of NV^- and NV^0 centers engineered in nanodiamond (ND) particles of 20-40 nm size were studied, aiming at development of a novel type of ND markers that are sensitive to chemical and electrical charge environment. It was found that NV^- luminescence was strongly reduced for the H-terminated ND surface compared with oxidized diamond. The original NV^-/NV^0 ratio could be restored by the annealing of ND in air at 400°C. All (ND and SCD) data support our model that the

surface band bending can influence strongly the NV^- and NV^0 luminescence in ND particles. The charge interactions scale as~ $1/r^2$ as confirmed by mathematical modeling. The NV^- and NV^0 luminescence in ND was compared with high quality SCD implanted by N^+ ions in a surface nano-layer. We clearly see that the PL enhancement by ND size effect and by the efficiency of conversion of N to NV centers compared to SCD diamond. In our case PL changes are visible even for particles of size of 40 nm. For small particles even the NV^0 luminescence can be fully quenched due to stronger band bending. This effect brings new possibilities for molecular imaging using ND, complementing the FRET technique.

We foresee that the observed effects of NV^- PL quenching at diamond surfaces can serve for optical monitoring of the chemical environment and biomolecular interactions close to the surface of ND particles by chemically induced electrical fields. Recently we have applied the presented effect of NV shifts by attaching charged polymer macromolecules[36] for real-time imaging in liquid for the case of fluorinated and hydrogenated ND. Molecular recognition events in cells are currently studied by our group.

Materials and methods

Materials

Sulfuric, nitric and hydrochloric acid and sodium hydroxide were purchased from Penta (Czech Republic) in p. a. purity. High pressure high temperature (HPHT) type Ib ND of 40-50 nm size, sourced from Microdiamant AG, Switzerland (size selected from commercial product MSY 0-0.05 GAF) contained about 200 ppm nitrogen. SCD CVD type IIa of high purity and, $3\times3\times0.5$ mm size, was purchased from Element 6.

Preparation of nanodiamond and diamond samples

A commercial solution of ND was lyophilized and heated in the slow stream of air at 425°C for 5 h to remove any sp^2 carbon-containing layer[37]. The resulting pale grey powder was dispersed in water and deposited in the form of a thin film on a target backing (10 mg cm^{-2}) for proton implantation. The ND

was then irradiated using an external proton beam of the isochronous cyclotron U-120M. The angle of the target backing with respect to the beam direction was 10°. The fluency of the delivered beam was 9.2×10^{15} cm^{-2}, beam energy 5.4 MeV and beam current 0.6 μA. The irradiated ND was thermally annealed *in vacuo* at 710°C for 2 h and then oxidized in a mixture of concentrated H_2SO_4-HNO_3 (9:1, vol/vol)[3] at 90°C for 7 days. The reaction mixture was diluted by deionized water, the NDs were separated by centrifugation and washed subsequently by 0.1 M NaOH, 0.1 M HCl, and finally three times by water. The solution was lyophilized providing highly luminescent NDs in the form of a stable colloidal dispersion in water as confirmed by AFM and DLS (final size ~20-40 nm). The colloidal dispersion was stable after 2 months with no sedimentation. A micro droplet of the dispersion was dried on a quartz substrate, producing isolated ND particles, as confirmed by AFM (see Figure S1 in Supplementary Material).

A SCD was irradiated with a N^+ ion beam using a low energy duoplasmatron ion-source. The energies of the nitrogen ions were 1 keV and 6 keV with a fluency of 10^{13} cm^{-2}, yielding a total concentration of N in the range of 100's ppm per exposure as simulated by TRIM[38] (Figure 6a). The mean projected range in diamond was 3 nm (1 keV) and 10 nm (6 keV). First we carried out implantation using 1 keV with half of the SCD covered by a mask, after this implantation we turned the crystal by 90° and implanted 6 keV ions, resulting in four different implantation sectors on one SCD (Figure 6). The implanted SCD was annealed *in vacuum* at 700°C for one hour, to create NV centres[39,40]. SCD was then oxidized by exposing it to H_2SO_4 and HNO_3 mixture using the same procedure as for the ND.

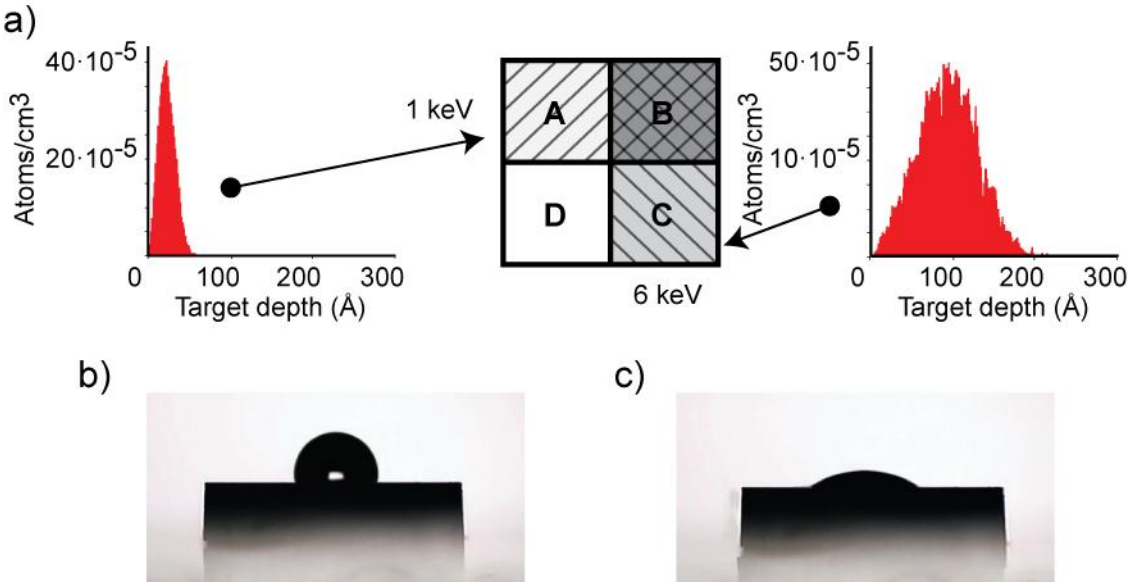

Figure 5. a) Schematic map and TRIM simulation for SCD diamond with four sectors implanted by N^+ ions. Sectors A and B were implanted with the same dose 10^{13} cm^{-2}, but different energies (1 and 6 keV, respectively). Sectors C and D were implanted twice at the same conditions (dose 10^{13} $cm^{-2,}$ energies 1 and 6 keV, respectively). The y-axis scale shows implanted atoms in atoms/cm^3 per 1 carbon atom. b) Contact angle of hydrogenated and c) oxidized SCD.

Surface treatment

Surface of ND and SCD was cleaned and oxidized after annealing by methods described above. Hydrogenation of samples was done in microwave-excited hydrogen plasma for 30 minutes at a temperature of 500°C and pressure of 1 mbar. Finally, the H-terminated samples were annealed for 120 minutes in air at 400°C to oxidize the surface. At each step the luminescence spectra were measured at room temperature.

The surface of the SCD after oxidation contained mainly carboxy, carbonyl, hydroxyl or lacton groups[41][41]. For the hydrogen terminated and oxidized SCD the surface contact angles were 92° and 18° respectively, confirming high efficiency of both hydrogen and oxidation treatments[42] (Figures 5b, c). The individual steps are summarized in Table 1.

Experimental	**Ib ND particles**	**IIa Single crystal CVD**

steps		
1) Implantation	Protons 5.4 MeV, $9.2x10^{15}$ atoms/cm^2	Nitrogen 1 and 6 keV, $6x10^{13}$ atoms/cm^2
2) Annealing	710°C, 2 hours, UHV	700°C, 2 hours, UHV
3) Oxidation	H_2SO_4 + HNO_3 (9:1) 90°C, 7 days	H_2SO_4 + HNO_3 (9:1) 90°C, 7 days
4) Hydrogenation	hydrogen plasma 30 minutes, 500°C, 1 mbar	hydrogen plasma 30 minutes, 500°C, 1 mbar
5) Oxidation	Annealing in air 400°C, 120 minutes	H_2SO_4 + HNO_3 (9:1) 90°C, 7 days

Table 1. The summarization of individual procedures within the experiment.

Luminescence measurements

The effects of surface termination on PL of NV centers were studied in two different configurations, using either nanodiamond (ND) particles[43-45][36] or single crystal diamond (SCD). The luminescence of individual particles was detected by a confocal microscope Olympus FV-1000, excitation wavelength 553 nm, laser power 15 mW. Raman and luminescence spectra were measured at Renishaw InVia Raman Microscope; excitation wavelength was 514 nm with 25 mW laser power. Spectra were taken at room temperature and normalized to the diamond Raman peak. The AFM measurements were performed in tapping mode (111 kHz) with an NTEGRA Prima NT MDT system equipped with a soft HA_NC etalon tip.

For measurements of luminescence changes upon consecutive annealing of hydrogenated ND in air, samples were heated to the target temperature (using a ramp of 25°C per minute), kept at the set temperature for 30 minutes and then cooled down to the room temperature. At each step the luminescence spectra were measured at room temperature.

ACKNOWLEDGMENT Special thanks to Dr. Jana Poltierova-Vejpravova for annealing the sample and to Dr. Ivan Gregora for help with Raman spectroscopy, to Prof. Joerg Wrachtrup, Prof. Fedor Jelezko and Dr. Friedenman Reinhard from Stuttgart University and to Jan Richter and Dr. Jan Svoboda for the help with confocal microscopy. The authors acknowledge the financial support from the Academy of Sciences of the Czech Republic (grants KAN200100801, KAN301370701 & KAN400480701), the European R&D projects (FP7 ITN Grant No. 238201 – MATCON, No. 245122 DINAMO and COST MP0901 – LD 11076 and LD11078), and MSM6840770012 "Transdisciplinary Research in the Field of Biomedical Engineering II".

Supporting Information Available:

Detailed description of the mathematical model of surface band bending including used equations, parameters and constants, figure showing the AFM picture of nanodiamonds used in the experiment, and surface conductivity measurements on the single crystal diamond with additional discussion connected to its influence on surface band bending are available free of charge via the Internet at http://pubs.acs.org.

References

[1] Ho, D; Beyond the Sparkle: The Impact of Nanodiamonds as Biolabeling and Therapeutic Agents, *ACS Nano*, **2009**, 3 (12), 3825–3829

[2] Fu, C.C; Lee, H.Y; Chen, K.; Lim, T.S; Wu, H.Y.; Lin, P.K.; Wei, P.K.; Tsao, P.H.; Chang, H.C; Fann, W. Characterization and application of single fluorescent nanodiamonds as cellular biomarkers. *Proc. Natl. Acad. Sci. USA* **2007**, 104 (3) 727-732

[3] Chang, Y.R.; Lee, H.Y; Chen, K.; Chang C.C; Tsai D.S; Fu, C.C; Lim T.S.; Tzeng Y.K.; Fang, C.Y.; Han C.C.; Chang, H.C.; Fann, W. “Mass production and dynamic imaging of fluorescent nanodiamonds”, *Nat. Nanotechnol.* **2008**, 3, 284 - 288

[4] Liu, K.K.; Cheng, C.L.; Chang, C.C.; Chao, J.I; Biocompatible and detectable carboxylated nanodiamond on human cell. *Nanotechnology* **2007**, 18, 325102

[5] Tisler, J; Balasubramanian, G; Naydenov, B; Kolesov, R; Grotz, B; Reuter, R; Boudou, J.B; Curmi, P.A; Sennour, M; Thorel, A et al; Fluorescence and Spin Properties of Defects in Single Digit Nanodiamonds. *ACS Nano*, **2009**, 3 (7), 1959–1965

[6] Gaebel, T.; Domhan, M.;Wittmann, C.; Popa, I.; Jelezko, F.; Rabeau, J.; Greentree, A.; Prawer, S.; Trajkov, E.; Hemmer, P.R.; Wrachtrup, J.; Photochromism in single nitrogen-vacancy defect in diamond. *Appl. Phys. B.* **2006**, 82, 243-246

[7] Iakoubovskii, K.; Adriaenssens, G. J.; Nesladek, M. Photochromism of vacancy-related centres in diamond, *J. Phys.:Cond. Matter*, **2000**, 12, 189-199

[8] Yu, S. J; Kang, M. W; Chang, H. C; Chen, K. M; Yu, Y. C; Bright fluorescent nanodiamonds: no photobleaching and low cytotoxicity *J. Am. Chem. Soc.* **2005**, 127 17604–5

[9] Yuan, Y.; Chen, Y.; Liu, Y.H.; Wang, H.; Liu, Y.; Biodistribution and fate of nanodiamonds in vivo. *Diamond Relat. Mater.*, **2009**, 18, 95–100

[10] Liang, Y; Ozawa, M; Krueger, A; A General Procedure to Functionalize Agglomerating Nanoparticles Demonstrated on Nanodiamond, *ACS Nano*, **2009**, 3 (8), 2288–2296

[11] Zhang, X.Q; Chen, M; Lam, R; Xu, X; Osawa, E; Ho, D; Polymer-Functionalized Nanodiamond Platforms as Vehicles for Gene Delivery. *ACS Nano*, **2009**, 3 (9), 2609–2616

[12] Faklaris, O; Joshi, V; Irinopoulou, T; Tauc, P; Sennour, M; Girard, H; Gesset, C; Arnault, J.C; Thorel, A; Boudou, J.B; Curmi, P.A; Treussart, F; Photoluminescent Diamond Nanoparticles for Cell Labeling: Study of the Uptake Mechanism in Mammalian Cells, *ACS Nano*, **2009**, 3 (12), 3955–3962

[13] Huang, H; Pierstorff, E; Osawa, E; Ho, D; Protein-Mediated Assembly of Nanodiamond Hydrogels into a Biocompatible and Biofunctional Multilayer Nanofilm, *ACS Nano*, **2008**, 2 (2), 203–212

[14] Martn, R; lvaro, M; Herance, J.R; Garca, H; Fenton-Treated Functionalized Diamond Nanoparticles as Gene Delivery System, *ACS Nano*, **2010**, 4 (1), 65–74

[15] Chen, M; Pierstorff, E.D; Lam, R; Li, S.Y; Huang, H; Osawa, E; Ho, D; Nanodiamond-Mediated Delivery of Water-Insoluble Therapeutics, *ACS Nano*, **2009**, 3 (7), 2016–2022

[16] Liu, K.K.; Zheng, W.W.; Wang, C.C.; Chiu, Y.C.; Cheng, C.L.; Lo, Y.-S.; Chen, C.; Chao, J.I.; Covalent linkage of nanodiamond-paclitaxel for drug delivery and cancer therapy. *Nanotechnology*, **2010**, 21 315106

[17] Davies, G; Hamer, M. F; Optical studies of the 1.945 eV vibronic band in diamond, *Proc. R. Soc. Lond. A.* , **1976**, 348, 285-298

[18] Lawson, S. C; Fisher, D; Hunt, D. C; Newton, M. E; On the existence of positively charged single-substitutional nitrogen in diamond, *J. Phys.: Condens. Matter*, **1998**, 10, 6171–6180

[19] Mohan, N; Tzeng, Y. K; Yang, L; Chen, Y. Y; Hui, Y. Y; Fang, C. Y; Chang, H. C; Sub-20-nm Fluorescent Nanodiamonds as Photostable Biolabels and Fluorescence Resonance Energy Transfer Donors, *Adv. Mater.* **2010**, 22, 843–847

[20] Hauf, M. V.; Grotz, B.; Naydenov, B.; Dankerl, M.; Pezzagna, S.; Meijer, J.; Jelezko, F.; Wrachtrup, J.; Stutzmann, M.; Reinhard, F.; Garrido, J. A.; Chemical control of the charge state of nitrogen-vacancy centers in diamond; in press, available online, arXiv; 1011.5109v2

[21] Nesladek, M.; Rezacova, V.; Kovalenko, A.; Kratochvilova, I.; Kocka, V.; Nanodiamond colour centres for cell-marker applications, EMRS Spring Meeting, Strasbourg, June 2010, Online:

http://www.emrs-strasbourg.com/files/USB%2010/symposium_d.pdf

[22] Ristein, J; Riedel, M; Ley, L; Electrochemical surface transfer doping – The mechanism behind the surface conductivity of hydrogen-terminated diamond, *J. Electrochem. Soc.*, **2004**, 151, 10,315-321

[23] Maier, F.; Riedel, M.; Mantel, B.; Ristein, J.; Ley, L.; Origin of surface conductivity in diamond, *Phys. Rev. Lett*., **2000**, 16, 85, 3472-3475

[24] Nebel, C.E.; Kato, H.; Rezek, B.;Shin, D.; Takeuchi, D.; Watanabe, H.; Yamamoto, T.; Electrochemical properties of undoped hydrogen terminated CVD diamond. *Diamond Relat. Mater.*, **2006**, 15, 264–268

[25] Nebel, C. E; Surface transfer-doping of H-terminated diamond with adsorbates, *New Diamond and Frontier Carbon Technology,* **2005**, 15, 5, 247-264

[26] Goss, J. P.; Briddon, P. R.; Jones, R.; Sque, S.; Donor and acceptor states in diamond. *Diamond Relat. Mater.*, **2004**, 13, 351–354

[27] Goss, J. P.; Briddon, P. R.; Jones, R.; Sque, S.; Rayson, M. J.; Vacancy-impurity complexes and limitations for implantation doping of diamond. *Phys. Rev. B*, **2005**, 72, 035214

[28] Kratochvilova, I.; Taylor, A.; Kovalenko, A.; Fendrych, F.; Rezacova, V.; Petrak, V.; Zalis, S.; Sebera, J.; Nesladek, M.; Fluoresent Nanodiamonds: Effect of Surface Termination, Mater. Res. Soc. Symp. Proc., 2010, 1203, J03-05.

[29] Fu, K.-M. C.; Santori, C.;Barclay, P. E.; Beausoleil, R. G. Conversion of neutral nitrogen-vacancy centers to negatively charged nitrogen-vacancy centers through selective oxidation. *Appl. Phys. Lett.*, **2010**, 96, 121907

[30] Nesladek, M; Stals, L.M; Stesmans, A; Iakoubovskij, K; Adriaenssens, G.J; Dominant defect

levels in diamond thin films: A photocurrent and electron paramagnetic resonance study. *Appl. Phys. Lett*., **1998**, 72, 25, 3306-3308

[31] Ristein, J.; Riedel, M.; Stammler, M.; Mantel B. F., Ley, L.; Surface conductivity of nitrogen-doped diamond. *Diamond Relat. Mater*., **2002**, 11, 359–364

[32] Rezek, B; Sauerer, C; Nebel, C.E; Stutzmann, M; Ristein, J; Ley, L; Snidero, E; Bergonzo, P; Fermi level on hydrogen terminated diamond surfaces, *Appl. Phys. Letters*, **2003**, 82, 14

[33] Pazzagna, S; Naydenov, B; Jelezko, F; Wratchup, J; Meijer, J; Creation efficiency of nitrogen-vacancy centres in diamond, *New Journal of Physics*, 2010, 12, 065017

[34] Santori, C; Barclay, P.E; Fu, K.C; Beausoleil, R.G; Vertical distribution of nitrogen-vacancy centers in diamond formed by ion implantation and annealing, *Phys. Rev. B*, **2009**, 79, 12, 5313-5321

[35] Boudou, J.P; Curmi, P.A; Jelezko, F; Wrachtrup, J; Aubert, P; Sennour, M; Balasubramanian, G; Reuter, R; Thorel A; Gaffet, E; High yield fabrication of fluorescent nanodiamonds, *Nanotechnology*, **2009**, 20, 23, 5602-5613

[36] Rezacova, V.; Nesladek, M.; Cigler, P.; Ledvina, M.; Kucka, J.; Stursa, J.; Ralis, J.; Vacik, J.; Mojzes, P.; Taylor, A.; Kratochvilova, I.; Fendrych, F.;On the Mechanism of Charge Transfer between Neutral and Negatively Charged Nitrogen-vacancy Color Centers in Diamond, MRS Fall Meeting, Boston, Nov.2010, Abstract No. A7.5 Online: http://www.mrs.org/s_mrs/doc.asp?CID=27791&DID=332936

[37] Osswald, S; Yushin, G; Mochalin, V;87 Kucheyev, S.O; Gogotsi, Y; Control of sp2/sp3 Carbon Ratio and Surface Chemistry of Nanodiamond Powders by Selective Oxidation in Air, *J. Am. Chem. Soc.*, **2006**, 128, 11635-11642

[38] Zeigler, J; The stopping range of ions in matter, SRIM-2008, online: http://srim.org

[39] Allers, L; Collins, A.T; Hiscock, J; The annealing of interstitial-related optical centres in type II natural and CVD diamond, *Diam. Relat. Mater.,* **1998**, 7 228–32

[40] Iakoubovskii, K; Adriaenssens, G.J; Trapping of vacancies by defects in diamond *J. Phys.: Condens. Matter*, **2001**, 13 6015–18

[41] Cigler, P; Ledvina, M; Tvrdonova, M; Rezacova, V; Nesladek, M; Kratochvilova, I; Fendrych, F; Stursa, J; Kucka, J; Ralis, J; Fluorescent nanodiamonds: new platform for construction of chemo- and biosensors. *Abstr. 2nd International Conference, Conference proceedings, Nanocon 2010 Olomouc, Czech Republic, October 12-14, 2010*

[42] Ostrovskaya, L; Perevertailo, V; Ralchenko, V; Dementjev, A; Loginova, O; Wettability and surface energy of oxidized and hydrogen plasma-treated diamond films, *Diam. Relat. Mater.,* **2002,** 11, 3-6, 845-850

[43] Williams, O.A; Hees, J; Dieker, C; Jger, W; Kirste, L; Nebel, C.E; Size-Dependent Reactivity of Diamond Nanoparticles, *ACS Nano*, **2010**, 4 (8), 4824–4830

[44] Schrand, A.M; Hens, S.A.C; Shenderova, O.A; Nanodiamond Particles: Properties and Perspectives for Bioapplications, *Critical Reviews in Solid State and Material Sciences*, **2009**, 34, 1-2, 18-74

[45] Kreuger, A; The structure and reactivity of nanoscale diamond, *J. Materials and Chemistry*, **2008**, vol. 18, i. 13, p. 1485-1492

SYNOPSIS TOC

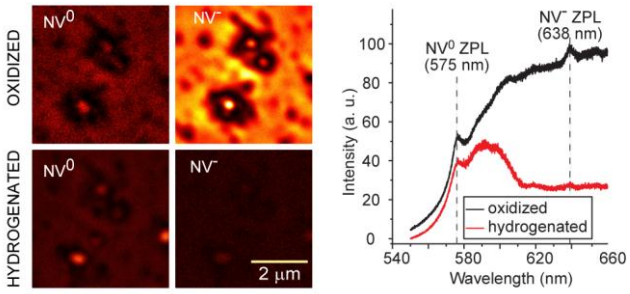

Supporting information

Details of mathematical model

To study quantitatively the occupation of NV^- and NV^0 ground states, we have carried out precise mathematical modeling outlined below.

The detail charge balance includes the surface acceptors at distance $x = 0$ with a surface density of 10^{13} cm^{-2} [S1]. For an H-terminated surface on a non-implanted SCD with the surface conductivity in the range of 10 kΩ, as measured in our case, we can assume that the Fermi level is pinned at the surface at EVBM [S2].

We can write for the depth (x) dependent total space charge density $\rho(x)$:

$$\rho(x) = eN_V \exp\left(-\frac{(E_F - E_V)_x}{kT}\right), \quad (1)$$

where N_V is the temperature dependent effective density of states at EVBM, $N_V = 2.7\times10^{19}\,cm^{-3}$ at room temperature, e is elementary charge, k is Boltzmann constant and T is thermodynamic temperature. E_F and E_V are energetic levels of Fermi and valence band.

$$\frac{d^2(E_F - E_V)_x}{dx^2} = \frac{e}{\varepsilon\varepsilon_0}\rho(x), \quad (2)$$

where $\varepsilon\varepsilon_0$ is the permittivity of material.

The Poisson equation was solved numerically with boundary conditions

$$(E_F - E_V)_0 = kT\ln\left(\frac{N_V}{p_0}\right) \quad (3)$$

$$p_0 = e\left(N_A - N_D(x)(1-\zeta) - N_D(x)\cdot\zeta\cdot g\right) \quad (4)$$

where p_0 is the total unscreened positive charge at $x = 0$ from (1) and N_A is the effective density of surface acceptors. The terms $e\,N_D(x)(1-\zeta)$ and $e\,N_D(x)\cdot\zeta\cdot g$ represent the net original concentrations of N and NV centers respectively in the sample before annealing. ζ is the conversion efficiency of N to NV centers for thermal annealing, which is different for SCD and for ND[S3,S4] g the relative occupation of NV^- and NV^0 centers in bulk diamond and the *e* the unitary electron charge. The concentration of nitrogen $N_D(x)$ is depth dependent. In the case of implanted SCD the density of donors (i.e. N and NV^- centers) is given by the TRIM simulation of the implantation N (Figure 6). For the case of HPHT NDs, we assume that nitrogen and NV centers are homogenously distributed in the sample thickness and the irradiation of 5.4 MeV protons is also homogenous in the volume. Only a part of the implanted nitrogen is converted to NV centers during annealing [S3, S4], therefore the parameter ζ is introduced to the model. This parameter represents a bulk dependent conversion efficiency of N in the lattice to NV centers. It has been shown recently[S3] that the parameter ζ depends strongly on the method of implantation, which can be also the reason for observed difference in the NV PL intensity in both SCD and HPHT ND, as discussed in the main text. In our calculations ζ was set to 0.1 for Ib HPHT NDs[S4] and 0.01 for IIa implanted and annealed SCD[S3]. Upon the annealing and diffusion of vacancies, one can estimate that N in the bulk of diamond will be proportionally converted to NV^0 and NV^- centers; therefore we introduce a parameter *g*, which is set in our standard stimulations to 0.5 (i.e. the concentration of NV^- and NV^0 centers would be equally produced without any surface bending). The deviation from the 0.5 value was discussed in ref.[S5]. Using these input parameters, the band bending was calculated.

To calculate the surface band bending in case of spherical symmetric ND particles, the above equations were transformed to spherical coordinates. The surface charge was assumed to be homogenously distributed at the surface of the sphere.

$$\frac{d^2(E_F - E_V)_r}{dr^2} = \frac{e}{\varepsilon\varepsilon_0} 4\pi e N_V \exp\left(-\frac{(E_F - E_V)_r}{kT}\right), \quad (5)$$

where r is the radius of the sphere. The boundary condition were used as previously.

AFM figure of ND particles

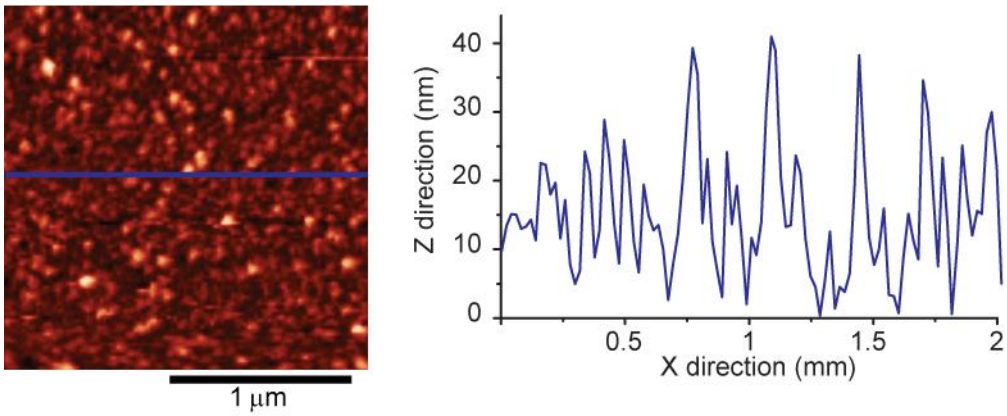

Figure. S1. AFM image of single dispersed ND particles, dispersed on a quartz glass.

Nitrogen content and surface conductivity

Surface conductivity measurements carried on implanted SCD. The non-implanted hydrogen terminated SCD showed low electrical resistivity (typically 10 kΩ), which is characteristic for 2-dimensional hole gas (2DHG) conductivity induced on H-terminated diamond surfaces by surface adsorbates[S2]. After implantation and subsequent hydrogen treatment, the resistivity of the N-implanted hydrogen terminated SCD increased, compared to non-implanted SCD to typically 80 kΩ - 2 MΩ when measured in various sectors. On the other hand, low surface conductivity can be caused by surface damage occurred due to implantation that has induced defects in the subsurface of the SCD. However, no such damage could be established by Raman spectroscopy, because sp^2 – carbon Raman lines are not visible in the spectra. This hypothesis is also neglected by the fact that on the sectors with higher implantation energies 6 keV, we could establish higher conductivity (80 kΩ) than in the sectors implanted with lower implantation energies of 1 keV. The 1 keV energy implantation leads to

generation of N-donors closer to the surface, as confirmed by the TRIM stimulations[S6]. The surface compensation effects seem to be the plausible explanation.

[S1] Nebel, C. E; Surface transfer-doping of H-terminated diamond with adsorbates, *New Diamond and Frontier Carbon Technology,* **2005**, 15, 5, 247-264

[S2] Maier, F.; Riedel, M.; Mantel, B.; Ristein, J.; Ley, L.; Origin of surface conductivity in diamond, *Phys. Rev. Lett*., **2000**, 16, 85, 3472-3475

[S3] Pazzagna, S; Naydenov, B; Jelezko, F; Wratchup, J; Meijer, J; Creation efficiency of nitrogen-vacancy centres in diamond, *New Journal of Physics*, 2010, 12, 065017

[S4] Boudou, J.P; Curmi, P.A; Jelezko, F; Wrachtrup, J; Aubert, P; Sennour, M; Balasubramanian, G; Reuter, R; Thorel A; Gaffet, E; High yield fabrication of fluorescent nanodiamonds, *Nanotechnology*, **2009**, 20, 23, 5602-5613

[S5] Santori, C; Barclay, P.E; Fu, K.C; Beausoleil, R.G; Vertical distribution of nitrogen-vacancy centers in diamond formed by ion implantation and annealing, *Phys. Rev. B*, **2009**, 79, 12, 5313-5321

[S6] Zeigler, J; The stopping range of ions in matter, SRIM-2008, http://srim.org